

Improving Voltage and Frequency Control of DERs through Dynamic Power Compensation

Rodrigo Bernal and Federico Milano

School of Electrical & Electronic Engineering, University College Dublin, Ireland

rodrigo.bernal@ucdconnect.ie, federico.milano@ucd.ie

Abstract—This work proposes a Dynamic Power Compensation (DPC) for the frequency and voltage controllers of converter-based Distributed Energy Resources (DERs) to improve the dynamic response of low-inertia power systems. The proposed approach adjusts both active and reactive powers of DERs to compensate the dynamic coupling between voltage and frequency controllers. This result is obtained by including additional signals to the standard controllers. These signals are defined based on the sensitivities of active and reactive powers with respect to bus voltage magnitudes and angles. Simulation results show an overall performance improvement in the power system when the proposed DPC is considered. Modified versions of the WSCC 9-bus and IEEE 39-bus benchmark systems are used to comprehensively assess the proposed DPC.

Index Terms—Low-inertia power systems, converter-interfaced generation, frequency control, voltage control.

I. INTRODUCTION

A. Motivations

Distributed Energy Resources (DERs) are typically connected to the grid through power electronic converters, providing additional flexibility and faster responses compared to conventional generators [1]. However, the substitution of conventional synchronous machines and controllers with devices whose dynamic interaction with the rest of the system is yet to be fully understood is one of the major challenges currently faced by system operators that aim at achieving net-zero targets [2], [3]. In this context, we propose a control strategy to enhance the overall dynamic performance of power systems. The proposed scheme exploits the dynamic cross-coupling between voltage frequency and magnitude with the DERs active and reactive power injections into ac grids.

B. Literature Review

In conventional power plants, the automatic voltage regulation and turbine governors are naturally decoupled by their time scales. In power electronic converters the Voltage Control (VC) and Frequency Control (FC) can have similar time scales but, in the same vein as conventional controllers, several control strategies to decouple FC and VC of converter-interfaced generation have been proposed. We cite, for example, the concept of virtual impedance control [4]; a modified

droop control based on an orthogonal power transformation [5] and [6]; a compensation for local load effects [7]; an adaptive virtual impedance to compensate for power variations [8], [9]; as well as a combination of virtual impedance and coupling compensation [10]. Although the controls above can effectively decouple the power flows, how to set the virtual impedance and/or compensation to ensure system stability has not been satisfactorily solved so far.

In this work, we adopt the opposite strategy, that is, we aim at designing a control that exploits – as opposed to reduce – the dynamic coupling between FC and VC converter-interfaced generation. There are in the literature several proposals also of this approach. The interdependence between FC and VC with active and reactive powers has been utilized to enhance power system frequency stability in [11]. Other approaches consist in utilizing active and reactive power in DFIGs to improve power system frequency stability [12]; adapting local voltage reference [13]; using smart loads reactive compensation to mitigate power fluctuations [14]; including voltage derivative in frequency recovery to improve system response [15], [16]. Cross feedbacks of active and reactive power controls have also been considered to enhance both FC and VC [17]. Nevertheless, how to fully avoid the negative effects of the FC-VC coupling that appears in these controls remains an unsolved question.

C. Contributions

We propose a control that exploits the dynamic coupling between FC and VC converter-interfaced generation. With this aim, we include a dynamic compensation in the active and reactive power loops of the DER controllers in order to improve the performance of FC and VC. The compensating signals are determined based on the sensitivities of active and reactive powers with respect to bus voltage magnitudes and angles at the point of connection of the DERs.

D. Paper Organization

The remainder of the paper is organized as follows. Section II provides the theoretical framework of the paper, that is, the derivation of the dynamic power compensation based on power flow equations, and applies the proposed compensation to the FC and VC of DER devices. Section III presents two case studies based on modified versions of the WSCC 9-bus and the IEEE 39 bus-system. Finally, conclusions and future work are given in Section IV.

This work is supported by Sustainable Energy Authority of Ireland (SEAI) by funding R. Bernal and F. Milano under project FRESLIPS, Grant No. RDD/00681.

II. PROPOSED DYNAMIC POWER COMPENSATION

We discuss first the coupling between voltage frequency and magnitude with active and reactive powers. To this aim, let us consider the active and reactive power injections in the branch connecting buses h and k :

$$\begin{aligned} P_{hk} &= v_h^2 G_{hh} + v_h v_k (G_{hk} \cos \theta_{hk} + B_{hk} \sin \theta_{hk}), \\ Q_{hk} &= -v_h^2 B_{hh} + v_h v_k (G_{hk} \sin \theta_{hk} - B_{hk} \cos \theta_{hk}), \end{aligned} \quad (1)$$

where P_{hk} and Q_{hk} are the active and reactive powers, respectively, injected in bus h flowing towards bus k , respectively; $G_{hh} + jB_{hh}$ and $G_{hk} + jB_{hk}$ are the diagonal h -th and (h, k) -th elements, respectively, of the grid admittance matrix; v_h and v_k represent the magnitude of the voltages at buses h and k , respectively; and $\theta_{hk} = \theta_h - \theta_k$ indicates the difference between voltage phase angles.

Equation (1) is valid for both steady-state and transient conditions. In the latter case, which is the relevant situation for control purposes and thus the focus of this paper, voltage magnitudes and angles are functions of time. Differentiation of (1) with respect to the angles and voltages gives:

$$\begin{aligned} dP_{hk} &= \underbrace{\frac{\partial P_{hk}}{\partial \theta_h} d\theta_h + \frac{\partial P_{hk}}{\partial \theta_k} d\theta_k}_{dP'_{hk}} + \underbrace{\frac{\partial P_{hk}}{\partial v_h} dv_h + \frac{\partial P_{hk}}{\partial v_k} dv_k}_{dP''_{hk}}, \\ dQ_{hk} &= \underbrace{\frac{\partial Q_{hk}}{\partial \theta_h} d\theta_h + \frac{\partial Q_{hk}}{\partial \theta_k} d\theta_k}_{dQ'_{hk}} + \underbrace{\frac{\partial Q_{hk}}{\partial v_h} dv_h + \frac{\partial Q_{hk}}{\partial v_k} dv_k}_{dQ''_{hk}}, \end{aligned} \quad (2)$$

where dP'_{hk} and dQ'_{hk} are the sensibilities of dP_{hk} and dQ_{hk} that depends on the angle. Accordingly, dP''_{hk} and dQ''_{hk} are the sensibilities of dP_{hk} and dQ_{hk} that depends only on the voltage.

For convenience of notation, let us rewrite (1) as:

$$\begin{aligned} P_{hk} &= \phi_{hh} + \phi_{hk} \\ Q_{hk} &= \psi_{hh} + \psi_{hk} \end{aligned} \quad (3)$$

where

$$\begin{aligned} \phi_{sr} &= v_s v_r (G_{sr} \cos \theta_{sr} + B_{sr} \sin \theta_{sr}), \\ \psi_{sr} &= v_s v_r (G_{sr} \sin \theta_{sr} - B_{sr} \cos \theta_{sr}). \end{aligned} \quad (4)$$

Then, the differential expressions for the active and reactive power components related to the angles are given by:

$$dP'_{hk} = -\psi_{hk} d\theta_{hk}, \quad (5)$$

$$dQ'_{hk} = \phi_{hk} d\theta_{hk}, \quad (6)$$

and, for the active and reactive power components related to the voltages, the differential expressions are given by:

$$dP''_{hk} = 2\phi_{hh} \frac{d(v_h)}{v_h} + \phi_{hk} \frac{d(v_h v_k)}{v_h v_k}, \quad (7)$$

$$dQ''_{hk} = 2\psi_{hh} \frac{d(v_h)}{v_h} + \psi_{hk} \frac{d(v_h v_k)}{v_h v_k}, \quad (8)$$

It is convenient to define the quantities:

$$\omega_r = \frac{d\theta_r}{dt} = \dot{\theta}_r, \quad \rho_r = \frac{1}{v_r} \frac{dv_r}{dt} = \frac{\dot{v}_r}{v_r}, \quad (9)$$

which are the instantaneous frequency deviation with respect to the synchronous reference and instantaneous bandwidth, respectively, of the bus voltage v_r . These quantities are estimated using basic Phased Locked Loops (PLLs) located at the local bus h and another at the remote bus k . ω_r and ρ_r can be combined to define the *complex frequency* of the voltage v_r as:

$$\bar{\eta}_r = \rho_r + j\omega_r. \quad (10)$$

The interested reader can find a comprehensive discussion on these quantities in [18]. y using (9) and dividing by dt , the expressions (5)-(8) can be reformulated as:

$$\dot{P}'_{hk} = -\psi_{hk} (\omega_k - \omega_h), \quad (11)$$

$$\dot{Q}'_{hk} = \phi_{hk} (\omega_k - \omega_h), \quad (12)$$

$$\dot{P}''_{hk} = 2\phi_{hh} \rho_h + \phi_{hk} (\rho_h + \rho_k), \quad (13)$$

$$\dot{Q}''_{hk} = 2\psi_{hh} \rho_h + \psi_{hk} (\rho_h + \rho_k). \quad (14)$$

To achieve perfect decoupling between FC and VC, it is crucial to ensure that there is no impact on voltage magnitude during FC and, *vice versa*, no impact on frequency while doing VC. This requires the complex quantities $dP'_{hk} + jdQ'_{hk}$ and $dP''_{hk} + jdQ''_{hk}$ to be orthogonal. One way to fulfill this condition is by setting the cross sensitivities dP''_{hk} and dQ'_{hk} to zero. However, achieving this ideal scenario in practice is challenging due to the strong coupling between voltage frequency, magnitude, and the active and reactive power injected to the grid. In the literature, thus, it has been proposed to minimizing one of these sensitivities at the expense of the other [13].

As anticipated in the introduction, in this work, rather than attempting to decouple active and reactive power controls, we exploits the coupling provided by the cross sensitivities dP''_{hk} and dQ'_{hk} . This coupling is utilized to enhance the active and reactive power controllers through an additional compensation in the active and reactive power channels of the DER controller.

Figure 1 illustrates the proposed control scheme, which includes an inner current control loop and an outer loop for FC and VC. Within the current control loop, the current components (i_d and i_q) are regulated in the dq -axis reference frame through a simple first-order transfer function. An anti-windup limiter ensures that these components remain within their specified limits. The FC loop takes the frequency error and applies a droop control and a parallel washout filter. Similarly, the voltage control loop adjusts the bus voltage using a Proportional-Integral (PI) controller and a parallel washout filter. The resulting outputs from the FC and VC are then combined with the active and reactive power references, respectively. Finally, for the active power channel, the term $K_f \cdot \Delta P''_{hk}$ is included, while for reactive power channel, the term $K_v \cdot \Delta Q'_{hk}$ is added. Here, K_f and K_v are gains used to regulate the DPC, $\Delta P''_{hk}$ and $\Delta Q'_{hk}$ represent the time integrals of the cross rates of change of powers \dot{P}''_{hk} and \dot{Q}'_{hk} given in (13) and (12), respectively.

To ensure consistent and effective support for FC and VC, an activation mechanism for the DPC is included to address

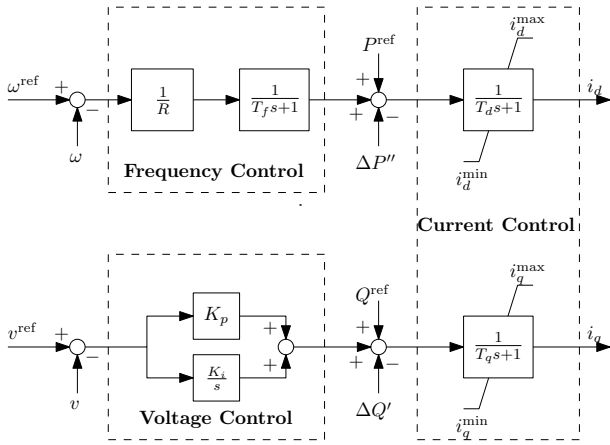


Fig. 1: Frequency and Voltage control loops with the inclusion of the proposed DPC in both active and reactive power references.

the possibility that the cross sensitivities dP''_{hk} and dQ'_{hk} may exhibit different signs depending on the system's dynamic. The compensation activation mechanism is formulated as follows:

$$K_f \cdot \Delta P''_{hk} = \begin{cases} K_f \cdot \Delta P''_{hk}, & \text{if } \Delta P''_{hk} \Delta P'_{hk} < 0 \\ 0, & \text{otherwise.} \end{cases}$$

$$K_v \cdot \Delta Q'_{hk} = \begin{cases} K_v \cdot \Delta Q'_{hk}, & \text{if } \Delta Q'_{hk} \Delta Q''_{hk} < 0 \\ 0, & \text{otherwise.} \end{cases} \quad (15)$$

Expression (15) works as a simple activation logic, triggering compensation when the signs of $\Delta P''_{hk}$ and $\Delta P'_{hk}$ are opposite in the case of FC, and when the signs of $\Delta Q'_{hk}$ and $\Delta Q''_{hk}$ are opposite in the case of VC.

The DPC activation mechanism ensures that active power compensation is considered only when variations in voltage magnitude have a negative impact on the FC's active power output. This mechanism also ensures that the reactive power compensation is triggered only if the frequency control is negatively affecting the VC's reactive power output.

We have chosen on purpose to use simple PI controllers for FC and VC. This allows easily replicating the results presented in the case study. However, any other more sophisticated transfer functions for the FC and VC controllers is fully compatible with the proposed DPC as long as the DER control consists of an inner and an outer loop.

III. CASE STUDY

This section presents simulation results based on modified versions of the WSCC 9-bus test system [19] (used for single DER testing) and the IEEE 39-bus benchmark [20] (used for multiple DER testing). In both systems, the SMs are represented by a 4th order (two-axis) model and are equipped with automatic voltage regulators and turbine governors.

The DERs are modelled as described in Section II. The parameters used for the DERs current, frequency and voltage controllers are presented in Table I. All DER controllers include current limiters. The DPC gains K_f and K_v are tuned per each DER of each network with the assistance of

eigenvalue sensitivity analysis, adjusting values by exploring an extensive range and combination of gains, and prioritizing those with high damping and assumed to remain unchanged in all scenarios. Null DPC gains, i.e., $K_f = K_v = 0$, corresponds to employing the conventional frequency and voltage control strategies.

TABLE I: Parameters of DER Controllers

Controller	Parameters
Current	$T_d = 0.6s, T_q = 0.6s$
Frequency	$R = 0.06, T_f = 1.2s$
Voltage	$K_i = 5, K_p = 10$

In all cases where a comparison with conventional control is carried out, the performance index μ proposed in [17] is calculated to undertake the combined effects of voltage magnitude and frequency. This index is obtained by integrating the magnitude of the complex frequency defined in (10) at a given bus r :

$$\mu_r(t) = \int_0^t |\bar{\eta}_r(\tau)| d\tau = \int_0^t \sqrt{\rho_r^2(\tau) + \omega_r^2(\tau)} d\tau. \quad (16)$$

The index in (16) was originally defined in [17] based on the concept of complex frequency proposed in [18]. This metric captures the combined effect of frequency and voltage controllers at the r -th bus. Since μ_r is a cumulative metric, the smaller its value, the more effective are these controllers.

Time domain simulations and small-signal analyses are used to study the performance of the proposed DPC. All results were obtained with the software tool Dome [21].

A. WSCC 9-bus System

In this section, we consider a modified version of the WSCC 9-bus system where we have replaced the Synchronous Machine (SM) located at bus 2 with a DER. The single-line diagrams of the modified system is shown in Fig. 2. The best setup of the DPC gains is found to be $K_f = 5$ and $K_v = 1$, which are the values utilized in all scenarios discussed in this section. Below, we illustrate the performance of the proposed DPC following a load outage and a fault; and discuss the effect of load models as well as of the parameters of DER controllers.

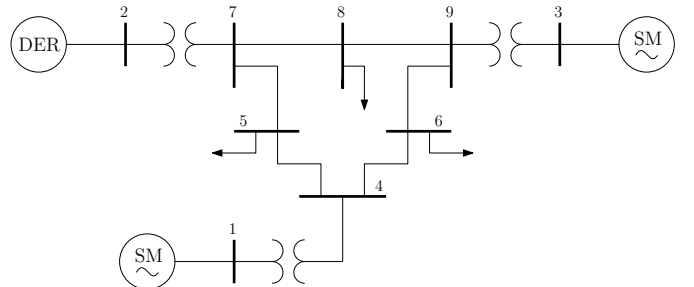


Fig. 2: Modified WSCC 9-bus system.

1) *Power Outage*: We consider first the outage of a load located at bus 5 of the WSCC 9-bus system. This contingency results in the loss of about 39% of the total system load. In this scenario, loads are modelled as constant impedance.

Figure 3 shows the frequency of the center of inertia (CoI) and the voltage magnitude at bus 2 following the load outage. The figure compares the conventional control ($K_v = K_f = 0$) and the proposed DPC approach ($K_v = 1, K_f = 5$). The plots indicate that the proposed DPC leads to a significant improvement in the overall dynamic behaviour of the frequency, without compromising the performance of the voltage control. This conclusion is confirmed by the performance index μ_2 shown in Fig. 4.

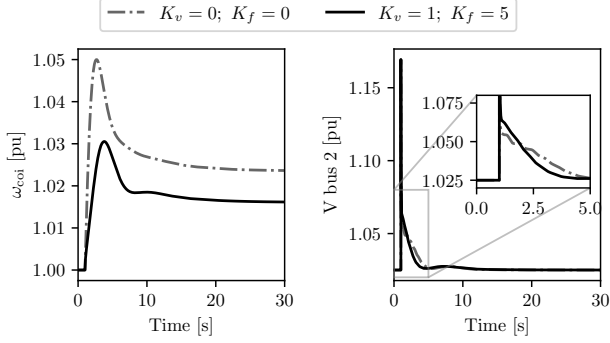


Fig. 3: Frequency of the CoI (left panel) and voltage (right panel) at bus 2 after the load outage at bus 5 for different control setups of the DER.

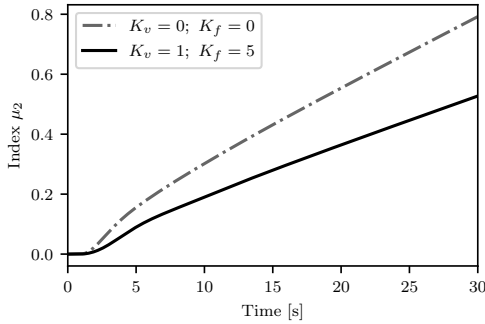


Fig. 4: Performance of the index μ_2 with and without DPC for the transient following the load outage at bus 5.

Figure 5 shows the behaviour of the variations in active and reactive powers injected by the DER without compensation ($K_v = K_f = 0$). To provide a better understanding of how the compensation operates in response to this specific contingency, these power injections are decomposed as $\Delta P'$ and $\Delta P''$ for active power, and $\Delta Q'$ and $\Delta Q''$ for reactive power. In this scenario, the signs of both $\Delta P''$ and $\Delta Q'$ are opposite to $\Delta P'$ and $\Delta Q''$. This makes the DPC effective to enhance both frequency and voltage controls of the DER.

2) *Three-phase Fault*: Next, we consider a three-phase balanced fault at bus 5 occurring at $t = 1$ s and cleared after 200 ms. Figure 6 shows the frequency of the CoI and the voltage magnitude at bus 2 following the fault. The plots compare the conventional control ($K_v = K_f = 0$) and the proposed DPC ($K_v = 1, K_f = 5$). Moreover, Fig. 7 shows the performance index μ_2 . The effect of the DPC is less pronounced than in the case of load outage. However, also

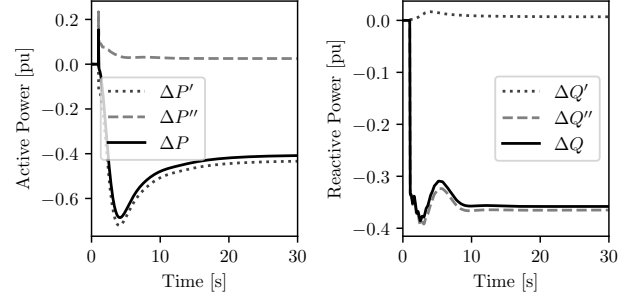


Fig. 5: Active (left panel) and reactive (right panel) decomposition during transient response after outage of load at bus 5 without DPC ($K_f = K_v = 0$).

in this scenario, the proposed DPC performs better than the conventional control.

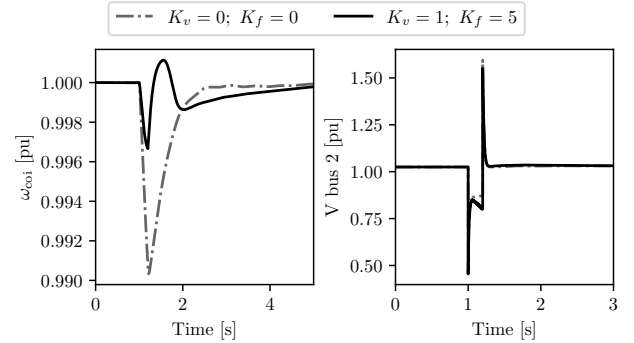


Fig. 6: Trajectories of the frequency of the CoI (left) and of the voltage at bus 2 (right) response following a fault at bus 5 with and without DPC.

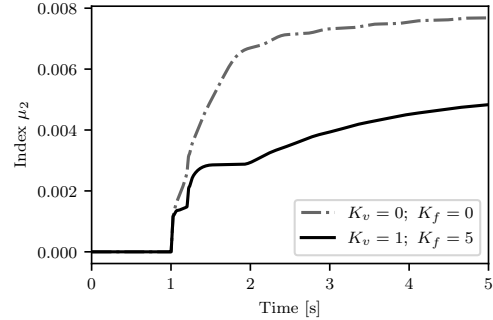


Fig. 7: Performance of the index μ_2 with and without DPC for the transient following a fault at bus 5.

The power signals employed for the DPC are shown in Fig. 8. As a three-phase fault predominantly impacts the voltage magnitude and the DPC is designed to address the cross-coupled effect between voltage magnitude and frequency, it is expected that the DPC mechanism will prioritize frequency control, as confirmed by the results shown in Fig. 6. Following the fault, the sign of $\Delta P'$ is opposite to that of $\Delta P''$, which indicates that the DPC is effective during this period. In particular, the magnitudes of $\Delta P''$ is reduced to a quarter of the value of $\Delta P'$ after the fault is cleared. This makes the proposed DPC to improve both the RoCoF and nadir of

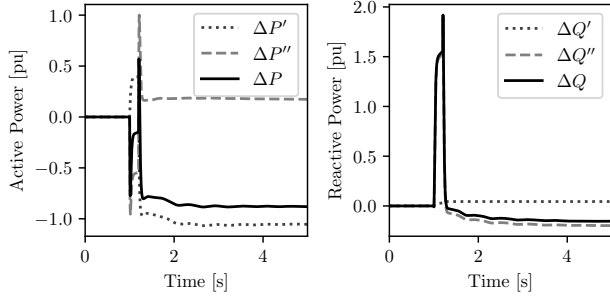


Fig. 8: Active (left panel) and reactive (right panel) power decomposition for the transient following a fault at bus 5.

the frequency when compared to the conventional frequency control. With regard to the reactive power compensation, even if the signal $\Delta Q'$ has opposite sign w.r.t. $\Delta Q''$, its magnitude is very small throughout the entire simulation. This results in the conventional and proposed control strategies to have a similar performance during the transient.

3) *Impact of Load Model:* As the load model can significantly impact the dynamics and coupling effects of voltage frequency and magnitude, it is important to analyze the performance of the DPC scheme under different load dynamics. To this aim, we consider three load models: constant power, constant current, and constant impedance. In all cases, the contingency is the load outage at bus 5.

Table II shows the simulation results and compares the proposed DPC scheme with the conventional approach. The performance metric utilized is μ_2 index calculated 30 s after the occurrence of the contingency. In the table, the values of the metric μ_2 are all normalized w.r.t. the value obtained for the constant power load model and the conventional control. Results indicate that, regardless the load model employed, the inclusion of the DPC scheme enhances the overall dynamic response of the system.

TABLE II: Normalized μ_2 index at 30 seconds for constant power, current and impedance load models.

Load Model	$\mu_2(30\text{ s})$	
	$K_v = K_f = 0$	$K_v = 1; K_f = 5$
Constant Power	1	0.54
Constant Current	0.95	0.59
Constant Impedance	0.91	0.62

4) *Sensitivity w.r.t. FC and VC Parameters:* In this subsection, a sensitivity in the FC and VC parameters is conducted. Particularly, the PI gains K_p and K_i for the voltage loop are changed to study the robustness of the DPC under different settings.

Figure 9 shows the performance index $\mu_2(10\text{ s})$ following a loss of load at bus 2 to capture faster dynamics related with the voltage. The index $\mu_2(10\text{ s})$ is parametrized with gains K_p and K_i , which are varied in the range $[1, 20]$. For comparison, Fig. 9 also shows the index μ_2 as obtained with the conventional DER control. The results indicate that

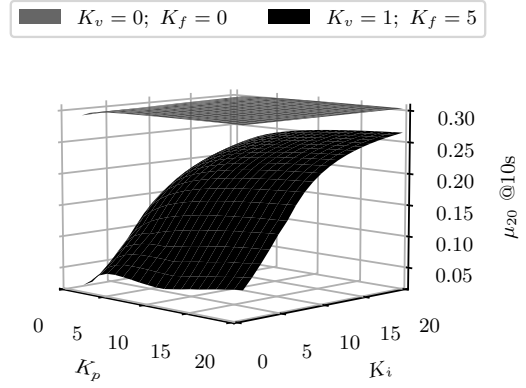


Fig. 9: Performance index $\mu_2(10\text{ s})$ for different voltage control PI gains K_i and K_p in the range $[1, 20]$.

regardless of the values of the controller gains, the proposed DPC consistently outperforms the conventional control in terms of overall dynamic performance.

B. New England 39-bus System

In this section, we consider a modified version of the IEEE 39-bus system where the SMs at buses 34, 35, and 37 have been replaced with DERs. To emulate a low inertia scenario, the inertias of the SMs 2-4, 7, 9 and 10 have been reduced by 30%, and the starting time of generator 1 has been reduced from 1000 s to 30 s. The parameters of the Power System Stabilizers (PSS) have been also adjusted to take into account the modified dynamics of the system and obtain a well damped dynamic response in the base case. The single-line diagram of the modified system is shown in Fig. 10.

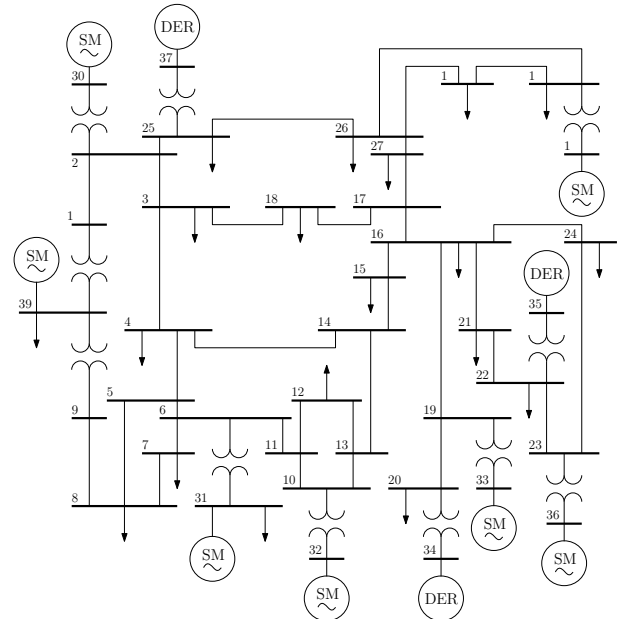


Fig. 10: Modified New England 39-bus system.

Three scenarios are considered, as follows:

- **Scenario 1 – Loss of generation:** Generator 4, representing about 10% of the total generation, is disconnected.

- **Scenario 2 – Loss of load:** The load located at bus 39, representing about 18% of the total load, is disconnected.
- **Scenario 3 – Fault:** A balanced three-phase fault located at bus 19 occurs at $t = 1$ s and is cleared after 200 ms.

Figure 11 shows the trajectories of the frequency of the CoI (left panels) and of the voltage magnitude at bus 20 (right panels), representing the HV terminal of DER, denoted as Gen 5 in Fig. 10). Additionally, Fig. 12 includes the performance index μ_{20} for three scenarios, comparing both conventional and proposed control strategies. Overall, the DPC is able to reduce both frequency and voltage magnitude variations compared to the conventional control.

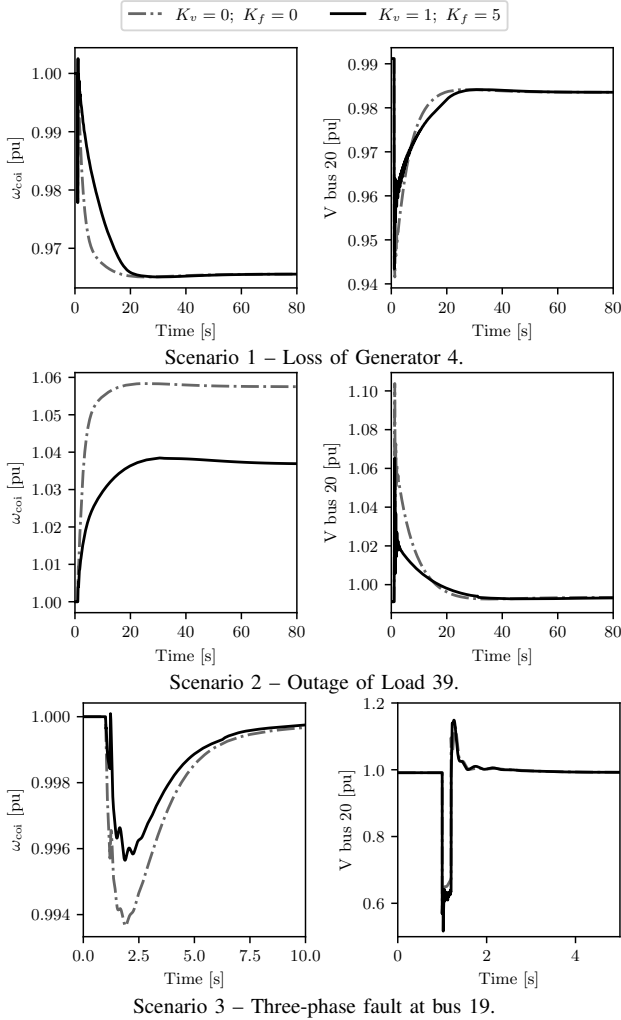
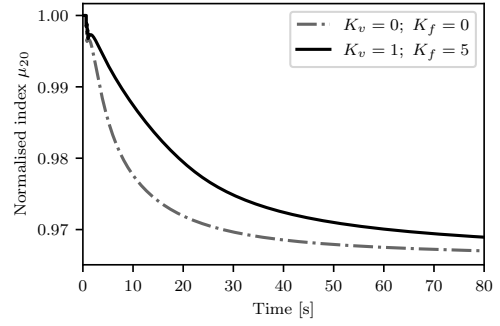
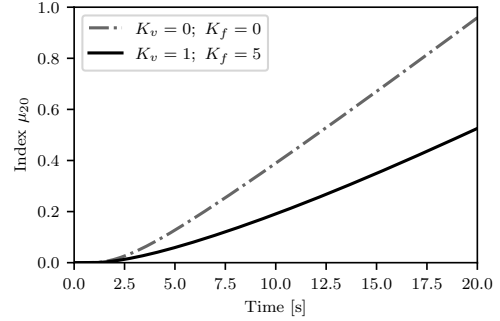


Fig. 11: Comparison of conventional control and proposed DPC for the modified New England 39-bus system.

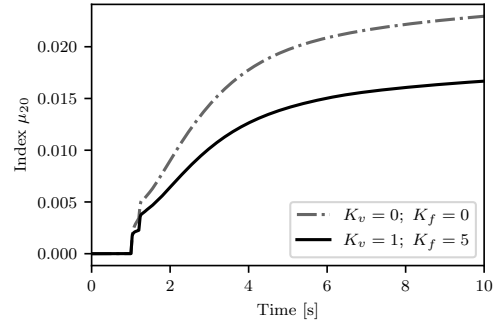
To better appreciate the effect of the DPC, Fig. 13 depicts the decomposition of active power and reactive power signals. The DPC is activated for frequency and voltage control when the signs of $\Delta P''$ ($\Delta Q'$) is opposite to $\Delta P'$ ($\Delta Q''$). This behaviour is exemplified in Scenario 1, where the signal $\Delta P''$ changes its sign at about $t = 20$ s, whereas $\Delta P'$ remains positive throughout the whole simulation. As a result, the active power compensation ceases, causing the frequency in



Scenario 1 – Loss of Generator 4.



Scenario 2 – Outage of Load 39.



Scenario 3 – Three-phase fault at bus 19.

Fig. 12: Performance index μ_{20} of the conventional control and of the proposed DPC based on the modified New England 39-bus system.

steady state to be determined by the droop characteristic of the frequency controller, just as the conventional approach. On the other hand, the DPC helps to reduce the RoCoF.

We note that, apart from the clear improvements in the dynamic behaviour of the system, the DPC can also introduce some small oscillations when compensating sudden jumps in voltage magnitude or angles. This effect can be appreciated in Scenario 3. These oscillations are generally small if the gains of the DPC are well tuned and can be substantially eliminated with additional filters in the DPC signals.

IV. CONCLUSIONS

The paper proposes a novel compensation approach, called DPC, that improves the overall dynamic response of power systems by including additional power signals into the active and reactive control channels of DERs. The DPC exploits the

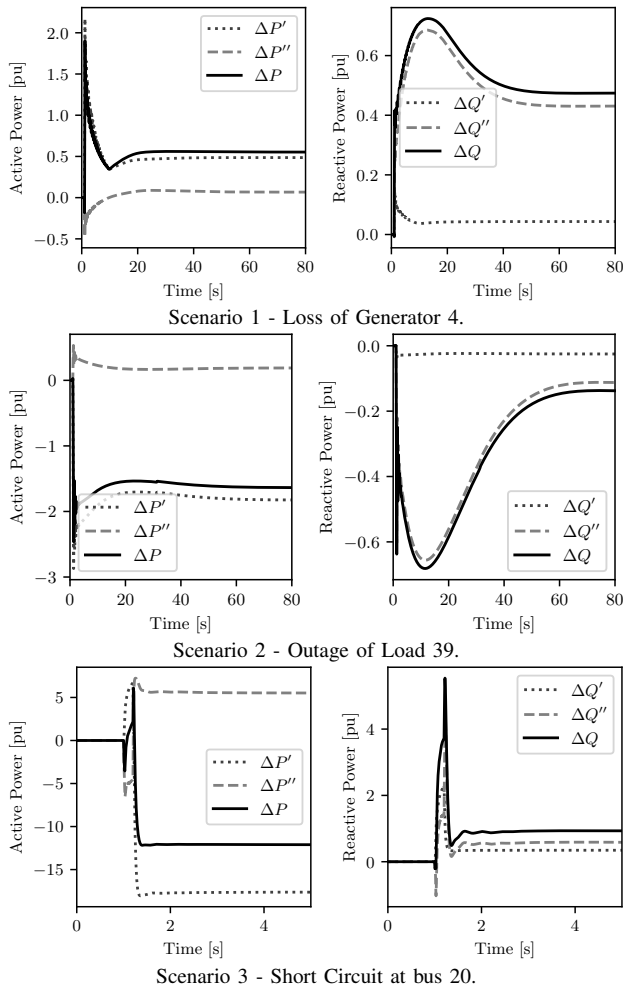


Fig. 13: Active (left panels) and reactive (right panels) decomposition with DPC enabled for the three scenarios of the modified New England 39-bus system.

inherent interdependence between voltage frequency, magnitude, and the active and reactive powers injected by the DERs.

The DPC is evaluated through analyzing local variations in voltage frequency and magnitude, as well as the response of the system's CoI frequency. The performance metric μ_i proposed in [17] is also utilized throughout the case study to compare the overall voltage/frequency variations obtained with the DPC and conventional DER control. Simulations consider various contingencies and parameters such as load models, control parameters, and low inertia conditions. Results show that the proposed DPC scheme consistently outperforms the conventional control approach in all scenarios, leading to significant improvements in the overall dynamic response of the system.

Future work will focus on improving the proposed DPC by further exploiting the coupled nature of voltage and frequency dynamics in low-inertia power systems. We also aim at comparing the performance of DPC with other control schemes proposed in the literature, i.e., virtual impedance control, and evaluate the effect of delays on the terms of the compensating signals that depends on remote measurements.

REFERENCES

- [1] P. Makolo, R. Zamora, and T.-T. Lie, "The role of inertia for grid flexibility under high penetration of variable renewables - a review of challenges and solutions," *Renewable and Sustainable Energy Reviews*, vol. 147, p. 111223, 2021.
- [2] F. Milano, F. Dörfler, G. Hug, D. J. Hill, and G. Verbić, "Foundations and challenges of low-inertia systems (invited paper)," in *2018 Power Systems Computation Conference (PSCC)*, 2018, pp. 1–25.
- [3] R. W. Kenyon *et al.*, "Stability and control of power systems with high penetrations of inverter-based resources: An accessible review of current knowledge and open questions," *Solar Energy*, vol. 210, pp. 149–168, 2020, special Issue on Grid Integration.
- [4] J. Guerrero, L. G. de Vicuna, J. Matas, M. Castilla, and J. Miret, "Output impedance design of parallel-connected ups inverters with wireless load-sharing control," *IEEE Transactions on Industrial Electronics*, vol. 52, no. 4, pp. 1126–1135, 2005.
- [5] K. De Brabandere, B. Bolsens, J. Van den Keybus, A. Woyte, J. Driesen, and R. Belmans, "A voltage and frequency droop control method for parallel inverters," *IEEE Transactions on Power Electronics*, vol. 22, no. 4, pp. 1107–1115, 2007.
- [6] Y. Li and Y. W. Li, "Power management of inverter interfaced autonomous microgrid based on virtual frequency-voltage frame," *IEEE Transactions on Smart Grid*, vol. 2, no. 1, pp. 30–40, 2011.
- [7] —, "Decoupled power control for an inverter based low voltage microgrid in autonomous operation," in *IEEE 6th Int. Power Electronics and Motion Control Conf.*, 2009, pp. 2490–2496.
- [8] H. Shi, F. Zhuo, H. Yi, F. Wang, D. Zhang, and Z. Geng, "A novel real-time voltage and frequency compensation strategy for photovoltaic-based microgrid," *IEEE Transactions on Industrial Electronics*, vol. 62, no. 6, pp. 3545–3556, 2015.
- [9] R. Sepshrad, M. Khojasteh Rahimi, A. Al-Durra, M. Allahbakhshi, and A. Moridi, "Optimal energy management of distributed generation in micro-grid to control the voltage and frequency based on PSO-adaptive virtual impedance method," *EPSR*, vol. 208, p. 107881, 2022.
- [10] Z. Peng, J. Wang, D. Bi, Y. Wen, Y. Dai, X. Yin, and Z. J. Shen, "Droop control strategy incorporating coupling compensation and virtual impedance for microgrid application," *IEEE Transactions on Energy Conversion*, vol. 34, no. 1, pp. 277–291, 2019.
- [11] M. Farrokhbabadi, C. A. Cañizares, and K. Bhattacharya, "Frequency control in isolated/islanded microgrids through voltage regulation," *IEEE Transactions on Smart Grid*, vol. 8, no. 3, pp. 1185–1194, 2017.
- [12] C. Tu, "A combined active and reactive power control strategy to improve power system frequency stability with DFIGs," *The Journal of Engineering*, vol. 2017, 11 2017.
- [13] G. Tzounas and F. Milano, "Improving the frequency response of ders through voltage feedback," in *2021 IEEE Power & Energy Society General Meeting (PESGM)*, 2021, pp. 1–5.
- [14] Z. Akhtar, B. Chaudhuri, and S. Y. Ron Hui, "Primary frequency control contribution from smart loads using reactive compensation," *IEEE Transactions on Smart Grid*, vol. 6, no. 5, pp. 2356–2365, 2015.
- [15] C.-T. Lee, C.-C. Chu, and P.-T. Cheng, "A new droop control method for the autonomous operation of distributed energy resource interface converters," *IEEE Transactions on Power Electronics*, vol. 28, no. 4, pp. 1980–1993, 2013.
- [16] K. W. Joung, T. Kim, and J.-W. Park, "Decoupled frequency and voltage control for stand-alone microgrid with high renewable penetration," in *2018 IEEE/IAS 54th Industrial and Commercial Power Systems Technical Conference (I&CPS)*, 2018, pp. 1–8.
- [17] W. Zhong, G. Tzounas, and F. Milano, "Improving the power system dynamic response through a combined voltage-frequency control of distributed energy resources," *IEEE Transactions on Power Systems*, vol. 37, no. 6, pp. 4375–4384, 2022.
- [18] F. Milano, "Complex frequency," *IEEE Transactions on Power Systems*, vol. 37, no. 2, pp. 1230–1240, 2022.
- [19] P. Sauer and M. Pai, *Power system dynamics and stability*. Prentice Hall, 1998.
- [20] Illinois Center for a Smarter Electric Grid (ICSEG), "IEEE 39-bus system," <http://publish.illinois.edu/smartergrid/ieee-39-bus-system/>.
- [21] F. Milano, "A Python-based software tool for power system analysis," in *IEEE PES General Meeting*, 2013, pp. 1–5.